Band structure of ^{68}Ge

D. Ward,[1] C. E. Svensson,[1,2] I. Ragnarsson,[3] C. Baktash,[4] M. A. Bentley,[5] J. A. Cameron,[2] M. P. Carpenter,[6] R. M. Clark,[1] M. Cromaz,[1] M. A. Deleplanque,[1] M. Devlin,[7,*] R. M. Diamond,[1] P. Fallon,[1] S. Flibotte,[2] A. Galindo-Uribarri,[4] D. S. Haslip,[2] R. V. F. Janssens,[6] T. Lampman,[2] G. J. Lane,[1] I. Y. Lee,[1] F. Lerma,[2] A. O. Macchiavelli,[1] S. D. Paul,[4] D. Radford,[4] D. Rudolph,[3] D. G. Sarantites,[7] B. Schaly,[2] D. Seweryniak,[6] F. S. Stephens,[1] O. Thelen,[8] K. Vetter,[1] J. C. Waddington,[2] J. N. Wilson,[2,†] and C.-H. Yu[4]

[1]*Nuclear Science Division, Lawrence Berkeley National Laboratory, Berkeley, California 94720*

[2]*Department of Physics and Astronomy, McMaster University, Hamilton, Ontario, Canada L8S 4M1*

[3]*Department of Physics, Lund University, P.O. Box 118, S-221 00 Lund, Sweden*

[4]*Physics Division, Oak Ridge National Laboratory, Oak Ridge, Tennessee 37831-6371*

[5]*School of Sciences, Staffordshire University, Stoke-on-Trent ST4 2DE, United Kingdom*

[6]*Physics Division, Argonne National Laboratory, Argonne, Illinois 60439*

[7]*Chemistry Department, Washington University, St. Louis, Missouri 63130*

[8]*Institut für Kernphysik, Universität zu Köln, D-50937 Köln, Germany*

(Received 19 June 2000; published 30 November 2000)

The nucleus ^{68}Ge has been studied by gamma-ray spectroscopy following its population at high spin in the reaction ^{40}Ca(^{32}S,4p)^{68}Ge. The reaction channel was selected with the Microball array and gamma rays were detected with the Gammasphere array. The level scheme is very complex, reflecting the many different, and presumably mixed, excitation modes in this nucleus. Nevertheless, there appear to be some simplifications in the spin range above $18\hbar$ where we have identified a superdeformed band and several terminating bands. The results are compared with a cranked Nilsson-Strutinsky model without pairing.

DOI: 10.1103/PhysRevC.63.014301 PACS number(s): 21.10.−k, 23.20.Lv, 25.70.Gh, 27.50.+e

I. INTRODUCTION

The development of large gamma detector arrays, together with very powerful ancillary detectors for light ions, has greatly increased the sensitivity of gamma-ray spectroscopy following heavy ion reactions of the type (HI,xn,yp,$z\alpha$). The techniques have been applied to study exotic nuclei in weakly populated reaction channels, and have allowed the study of very weak decay paths in nuclei produced in the dominant reaction channels. These nuclei may, with the very high sensitivity now achieved, reveal interesting aspects of nuclear structure. The recent observation of highly collective bands in nuclei just outside the double spherical shell closure at ^{56}Ni (cf. [1–5]) is of considerable interest, since this region has generally been considered to be described well by the spherical shell model. A motivation for the present work was to investigate how the addition of valence nucleons outside the ^{56}Ni core influences nuclear structure at high spin.

Previous experimental studies of the ^{68}Ge level scheme have been made by de Lima *et al.* [6], Chaturvedi *et al.* [7,8], and by Hermkens *et al.* [9].

II. EXPERIMENTAL

A target comprising a 500 μg/cm^2 foil of metallic ^{40}Ca flashed on both sides with 100 μg/cm^2 gold layers to prevent oxidation was bombarded by a 134 MeV ^{32}S beam delivered by the ATLAS accelerator at the Argonne National Laboratory. Here we discuss results for ^{68}Ge, populated via the four proton evaporation channel. This was one of the most strongly populated channels in the reaction, produced in approximately 20% of the fusion events.

For this experiment the Gammasphere array [10] contained 101 HPGe detectors. Light charged particles were detected with the Microball [11], a 4π array of 95 CsI(Tl) scintillators. Collimators normally in place to shield the BGO suppressors of Gammasphere from a direct view of the target were removed to enable gamma-ray multiplicity and total sum energy measurement [12]. Events were recorded when a trigger on fourfold (or higher) clean γ-coincidences in the Compton suppressed array was issued. Approximately 1.7×10^9 such events were recorded to magnetic tape.

The data for ^{68}Ge discussed here were analyzed with requirements that (1) four protons were detected in Microball, (2) the total energy of the detected protons plus the recoil energy of the nucleus in the center-of-mass frame, added to the total gamma energy detected, was consistent with that expected for the four-proton channel. This latter condition is simply an application of conservation of energy and serves to reduce contaminant events from other reaction channels in which one or more of the evaporated particles were not detected [13]. The selected events were decomposed into double coincidences and incremented into a symmetrized gamma-gamma coincidence matrix containing approximately 1.0×10^9 coincidences, over 95% of which were associated with ^{68}Ge. The only remaining contaminants that could be identified were ^{67}Ge ($4pn$), ^{67}Ga ($5p$), and ^{65}Ga ($\alpha3p$). The intensities of these contaminants relative

*Present address: Los Alamos National Laboratory, Los Alamos, NM 87545.

†Present address: Niels Bohr Institute, Blegdamsvej 17, Copenhagen, Denmark.

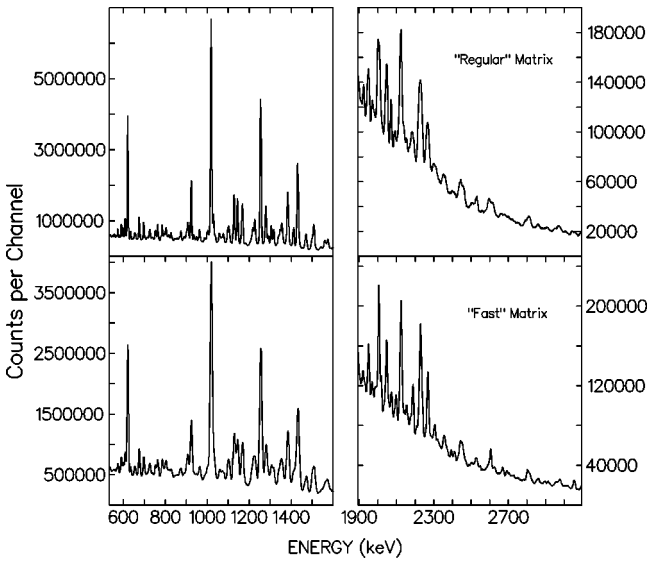

FIG. 1. Projections of the ''Regular'' $v/c=0.0357$, and ''Fast'' $v/c=0.0412$ matrices (see text).

to the ^{68}Ge $(4p)$ channel were estimated to be 1.0%, 1.1%, and 2.5%, respectively. The origin of these contaminants is clear; in the case of ^{67}Ge, a neutron was evaporated but the total energy registered (four detected protons plus the summed gamma-radiation) overlapped the region selected for the $4p$ channel, presumably because a higher than average fraction of the total gamma-energy happened to be detected for those events. Similarly, in the case of ^{67}Ga, one of the five evaporated protons was not detected, but the summed gamma-energy registered must have been higher than average. The leak through of the strong ^{65}Ga $(\alpha 3p)$ channel into the $4p$-gated data arose from the occasional misidentification of a low-energy alpha as a proton in detectors located at backward angles relative to the beam axis.

A correction to the mean recoil velocity according to the momentum vectors of the detected protons was applied to the gamma-ray energies on an event-by-event basis [14]. The bulk of the analysis was performed with the codes devised by Radford [15]. These codes were applied to a matrix in which the mean recoil velocity was taken to be 3.57% of light speed, *c*, appropriate to production at the midpoint of the target foil followed by γ decay after slowing down in, and exiting, the foil. This recoil velocity gave the best resolution for the majority of the transitions, where the state lifetimes were appreciably longer than a transit time through the foil (on the order of 100 fs). A second gamma-gamma matrix was constructed in which the recoil velocity was taken to be 4.12% of *c*, appropriate to production at the midpoint of the foil followed by γ decay in a negligible time compared to the foil transit time. This matrix gave the best resolution for gamma-rays emitted from very short-lived states in the terminating bands and in the superdeformed band. Projections of these matrices are shown in Fig. 1, where it is clear that higher-energy gamma rays (say $E \geqslant 1900$ keV) in the ''fast'' matrix are sharper than the corresponding peaks in the ''regular'' matrix, while the converse is true for lower-energy gamma rays.

A third gamma-gamma matrix was constructed for measuring the directional correlations of coincident gamma rays (sometimes called a DCO matrix). Events recorded in the angular range 79.2–100.8° (28 detectors of Gammasphere) were incremented along the *x* dimension, while events in the angular range 17.3–37.4°, and 142.6–162.7° (23 detectors) were incremented along the *y* dimension. As documented in the literature, e.g. [16], the intensity ratio of coincident pairs of gamma rays evaluated at coordinates $(x,y)/(y,x)$ give useful but limited assignments to transition multipolarities.

III. RESULTS

A. Low-spin level scheme

The low-spin level scheme derived in the present experiment is shown in Fig. 2. It is based on a detailed analysis of the gamma-gamma matrix with the RADWARE analysis package ESCL8R [15]. Spin assignments are based on analysis of the DCO matrix. Parity assignments to the levels at 3649 keV (5^-), 3883 keV (6^-), and 4054 (7^-) are those of previous work. Beyond that, we assume that levels decaying predominantly to negative parity levels have themselves negative parity. Tables of gamma-ray energies and intensities from this experiment are available on the world-wide web [17].

Previous studies by Chaturvedi *et al.* [7] and by de Lima *et al.* [6] used much less sensitive equipment; a more recent study by Hermkens *et al.* [9] produced a low-spin level scheme of comparable detail to our own. Of the 22 levels of negative parity, up to, and including $(15^-)E=8791$ keV shown in Fig. 2, 21 correspond with the scheme of Hermkens. The only point of difference concerns the ordering of $\gamma 983$ keV versus $\gamma 252$ keV. With our ordering, we place a (4^-) level at 2900 keV, whereas the reverse ordering of Hermkens *et al.*, puts the corresponding level at 3631 keV. A second experiment by Chaturvedi *et al.* [8] assigned some 19 levels of negative parity up to $E=8791$ keV, all of which correspond with our own assignments.

We have assigned 26 positive-parity levels up to spin $(12^+)E=7763$ keV, shown in Fig. 2. The level at 6663 keV has no correspondence in the scheme of Hermkens *et al.*, whereas their level at 3040 keV has no correspondence in our scheme; a level at 3041 keV is reported by de Lima. In the same excitation range, the later experiment of Chaturvedi *et al.* missed several positive parity levels assigned by ourselves and by Hermkens *et al*. Also, we find no evidence for the level at 6671 keV assigned by them.

B. High-spin level scheme

The level scheme at high spins, Fig. 3, was deduced from the regular gamma-gamma matrix with the RADWARE analysis package, but we have also made extensive use of the ''fast'' matrix. The only levels previously identified above excitation energy 8173 keV (13^-) in the study by Hermkens

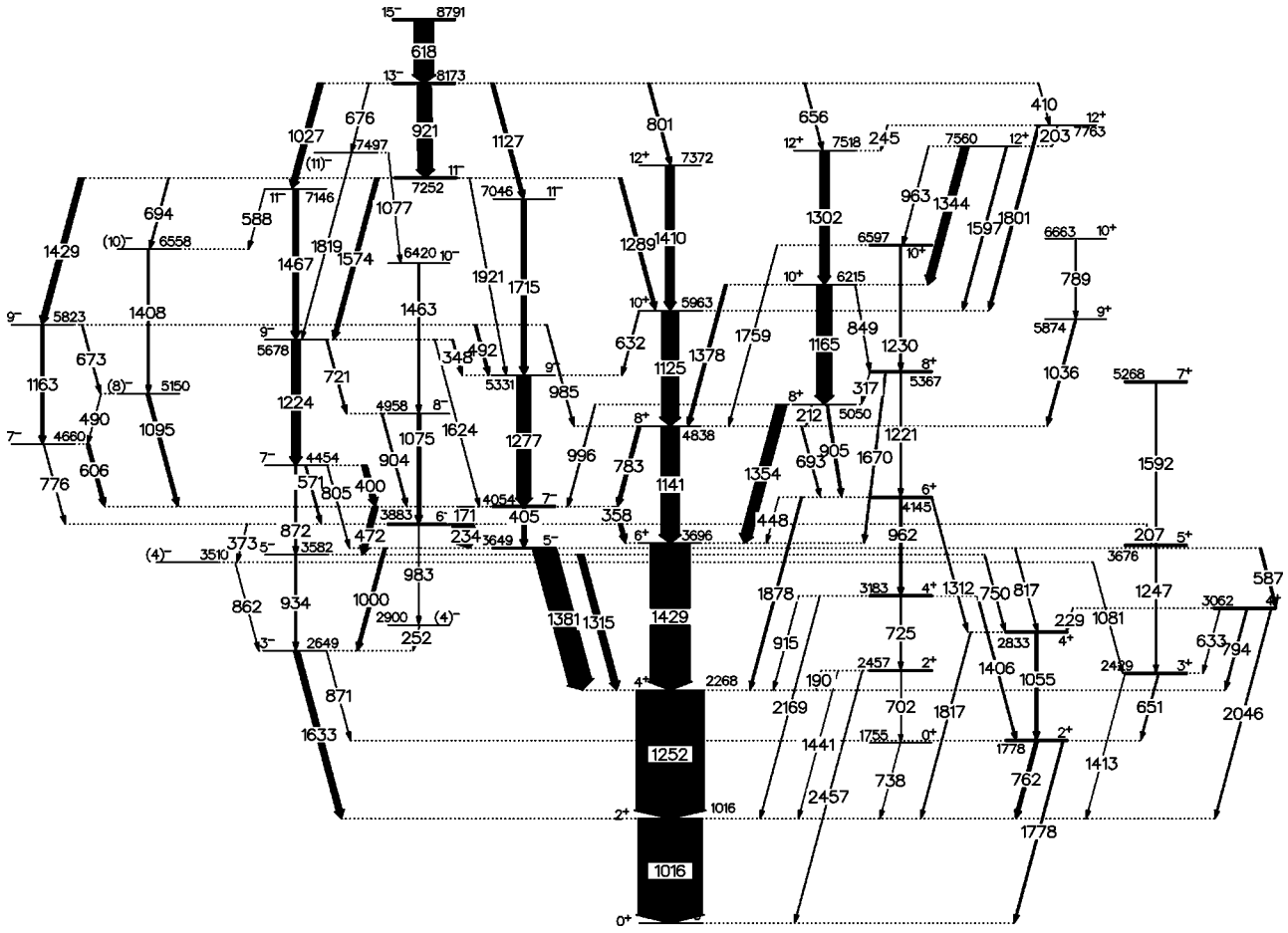

FIG. 2. Low-spin level scheme for ^{68}Ge from the present experiment.

et al. (using the present energies as labels), were 8792, 9389, and 10 297 keV for negative parity, and 8661, 8869, and 10 218 keV for positive parity. Their level at 10 075 keV was not seen in our data. Also, in this high-spin regime, levels at 8661, 9170, 9013, and 10 665 were proposed by Chaturvedi *et al.*, and correspond with our own assignments, whereas their levels at 8933, 9805, and 11 359 keV have no correspondence with our scheme, or with that of de Lima. The later experiment of Chaturvedi *et al.* assigns levels at 8662, 9014, 9171, and 10 664 keV in agreement with our level scheme, and levels at 8933, 8868, and 10 025 keV, which have no correspondence with our scheme. Figure 4 shows γ spectra in coincidence with the highest assigned transition in each of the high-spin bands observed in the present experiment.

IV. DISCUSSION OF THE LOW-SPIN STRUCTURE

The splitting of the yrast sequence into three 8^+ states is an interesting feature of the ^{68}Ge level scheme. In particle-plus-rotor calculations, de Lima *et al.* identified these states as $(\nu g_{9/2})^2(8^+_1)$, $(\pi g_{9/2})^2(8^+_2)$, and the continuation of the ground-state band as (8^+_3). In analyses based on generalized VAMPIR calculations [18], Chaturvedi *et al.* and Hermkens *et al.* identify the (8^+_3) as the continuation of the oblate ground state band, whereas the $(\nu g_{9/2})^2$ is assigned as 8^+_2. In these assignments, the measured g-factor, $g = -0.28 \pm 0.14$ for the 8^+_2 state [19] confirms its character.

The tight cluster of states at $3649(5^-)$, $3883(6^-)$, and $4054(7^-)$ keV are very strongly populated in the present experiment, they have the structure $\pi,\nu[p_{1/2},p_{3/2}, f_{5/2}\otimes g_{9/2}]$. In the two quasiparticle calculations of de Lima *et al.*, there are four low-lying negative-parity bands having one rotationally-aligned quasiparticle in $g_{9/2}$ (either ν or π) and one deformation-aligned quasiparticle in $p_{1/2}$, $p_{3/2}$, or $f_{5/2}$. In these calculations, the proton bands tend to be signature-split, whereas the neutron bands are not. Basing their argument mainly on this feature their assignments are of the 3649(5), 4054(7), 5331(9), and 7046(11) keV levels to the proton band (with negative parity): the neutron band is proposed to be 3582(5), 4454(7), 5678(9), and 7146(11) with negative parity. These authors also assign 3883(6) and 4958(8) as the signature partner to the neutron band. The present work extends the even-signature neutron band to 6420 keV (10^-), and 2900 keV (4^-). A second pair of signature partner bands beginning at 4660 keV(7^-), and 5150 keV(8^-) are proposed in the present level scheme.

The course of the five negative-parity bands discussed

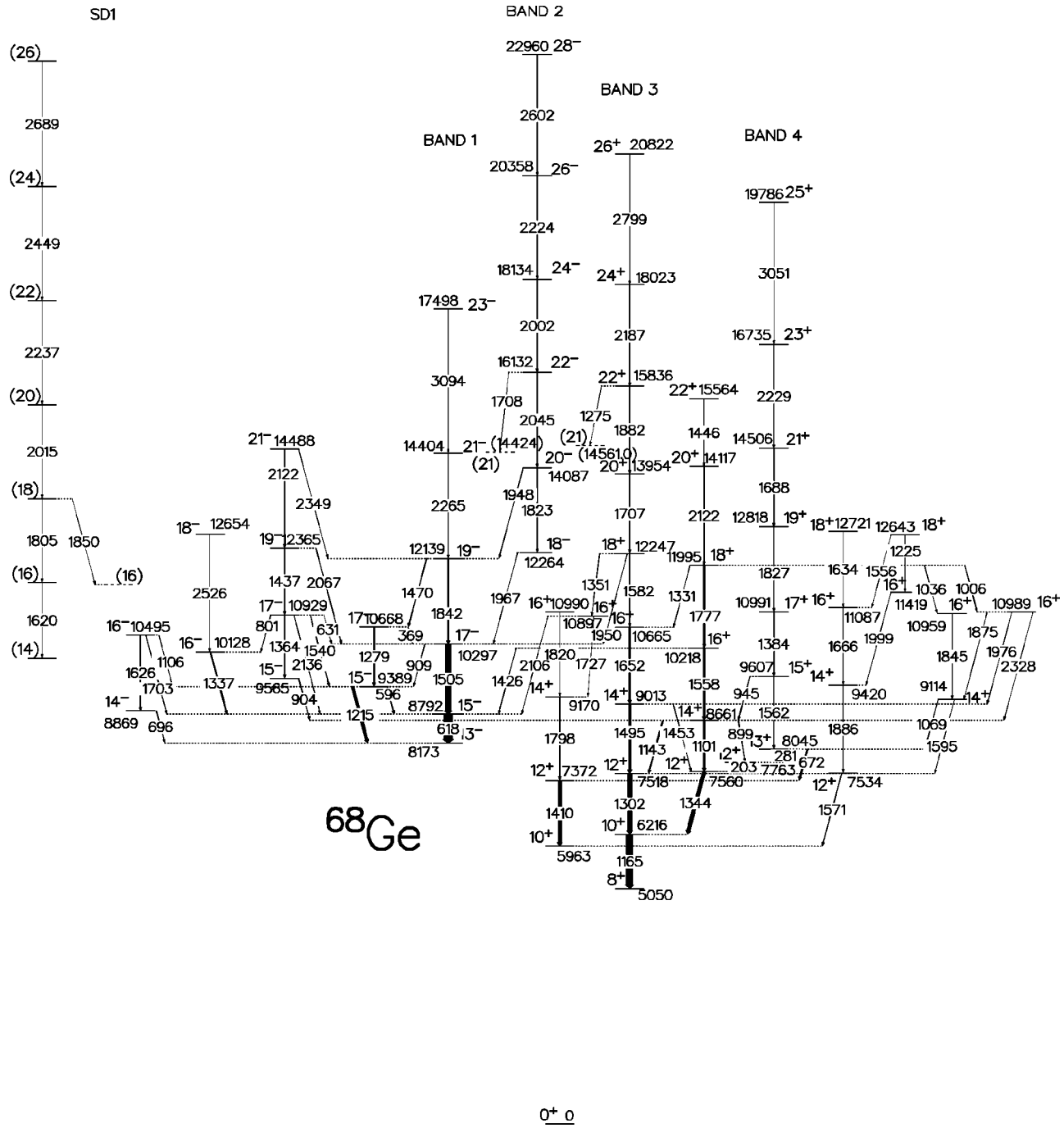

FIG. 3. High-spin level scheme for ^{68}Ge from the present experiment. The superdeformed band has not been linked to the level scheme and its position is schematic.

above is cut off by the occurrence of two very favored (low-lying considering their spin) negative-parity states 8173 keV(13^-) and 8790 keV(15^-). The low-lying negative-parity bands receive all their feeding from these two levels and none of their higher members can be identified reliably. Even the positive-parity bands receive population from the 13^- state, as seen in Fig. 2, but in this case there is also substantial feeding from higher lying positive parity states which allows us to extend the bands to higher spins.

V. CNS CALCULATIONS AT HIGH SPIN

Calculations have been carried out in the cranked Nilsson-Strutinsky (CNS) approach to try to understand the observed high-spin bands in ^{68}Ge. Configurations were fixed in a standard way used in recent band-termination calculations (cf. Ref. [20]). Following previous calculations in the $A=70-80$ mass region, e.g. [21,22], we have used the $A=80$ parameters of Galeriu *et al.* [23]. Pairing was neglected, which is a good approximation above spin 15–20 $\hbar$

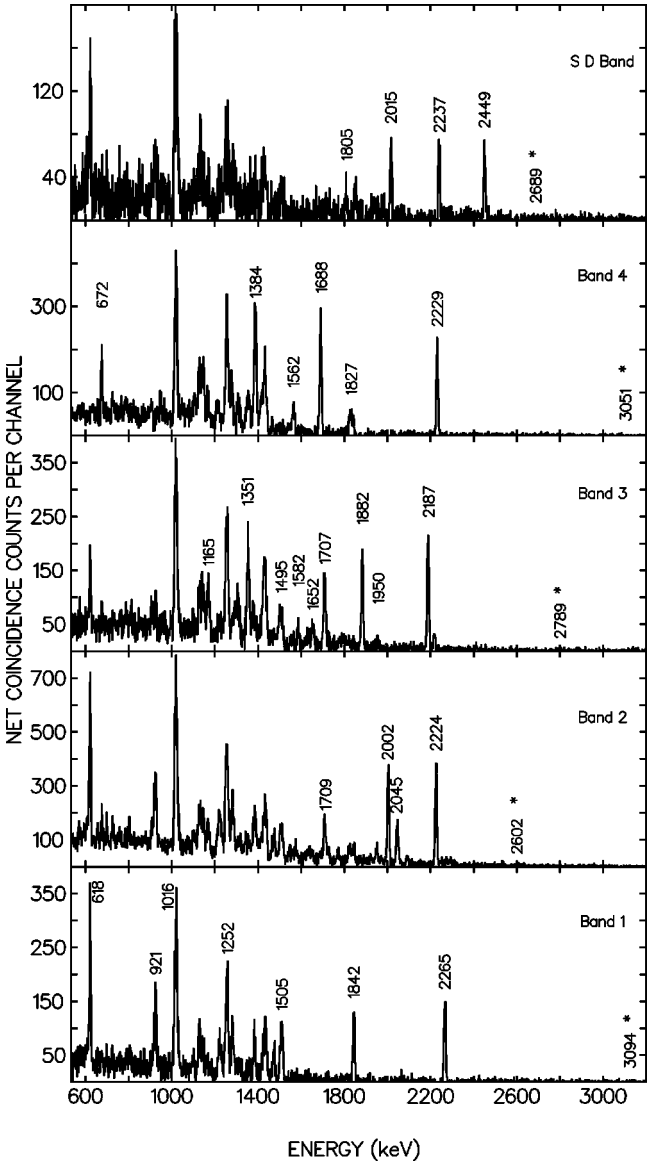

FIG. 4. Coincidence spectra gated on the topmost transition in each of the high-spin bands. Gamma-ray energies are given in keV, and the positions of the gating transitions are indicated.

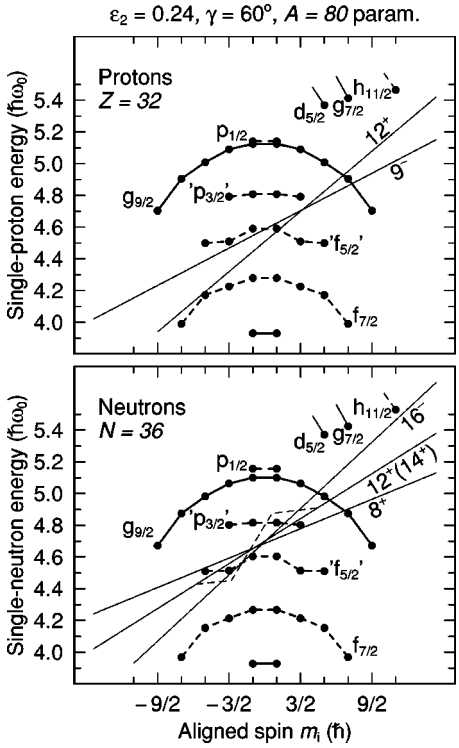

FIG. 5. The single-particle energies at an oblate deformation of $\varepsilon_2=0.24$ drawn versus their spin projection on the symmetry axis, m_i. The occupation of different orbitals in aligned configurations are illustrated by sloping Fermi surfaces. The highest spin states in bands 1–4 are interpreted as formed from the combination of the proton spins $I_p=12^+$ and 9^- with the neutron spins $I_n=16^-$ and 14^+. The proton spins 12^+ and 8^+ are used when forming aligned states at lower spin values in the configurations terminating at 23^- and 26^+.

in this mass region [20]. Reasonably regular high-spin bands are those observed to 23^-, 28^-, 26^+, and 25^+, labeled respectively bands 1 through 4 in Fig. 3, and the superdeformed band labeled SD1. Only these bands are considered here.

A. General considerations

The nucleus ^{68}Ge has four protons and eight neutrons outside the doubly magic core, ^{56}Ni. In the valence configurations, the active orbitals are those of the $N=3$ $p_{3/2}$, $f_{5/2}$, and $p_{1/2}$ subshells and the $N=4$ $g_{9/2}$ intruder subshell. Low-lying configurations will have one or two $g_{9/2}$ protons and two or three $g_{9/2}$ neutrons. The highest-spin state which can be formed in configurations of this kind is $I_p=12^+$ for the protons and $I_n=17^-$ for the neutrons, i.e., $I_{\max}=29^-$. Higher-spin states might be formed by exciting one or two protons from $f_{7/2}$, lying below the 28 shell gap, to the valence space orbitals. With one $f_{7/2}$ proton excited, we would expect signature partner bands connected by strong $M1$ transitions but no such bands were observed. As we will show later, the superdeformed band probably has two $f_{7/2}$ protons excited.

We label the configurations in a standard notation [21] by $[p_1\ p_2,\ n_1]$ where p_1 is the number of $f_{7/2}$ proton holes, p_2 the number of $g_{9/2}$ protons and n_1 the number of $g_{9/2}$ neutrons. The favored high-spin configurations with $p_1=0$ are then [01,2], [01,3], [02,2], [02,3]. With one or three $g_{9/2}$ particles, the favored signature for this subset is always $\alpha=+1/2$ while with an odd number of $(f_{5/2},p_{3/2})$ particles, the favored signature in prolate or near-prolate configurations is found to be $\alpha=1/2$ for three particles and $\alpha=-1/2$ for five particles. The specific occupation of the $f_{5/2}$ and $p_{3/2}$ orbits is illustrated in Fig. 5 from where the various $I_{\max}$ values can be derived:

$$\pi(g_{9/2})^1(f_{5/2},p_{3/2})^3 \Rightarrow I_{\max}=4.5+4.5=9^-,$$

$$\pi(g_{9/2})^2(f_{5/2},p_{3/2})^2 \Rightarrow I_{\max}=8+4=12^+,$$

$$\nu(g_{9/2})^2(f_{5/2},p_{3/2})^6 \Rightarrow I_{\max}=8+6=14^+,$$

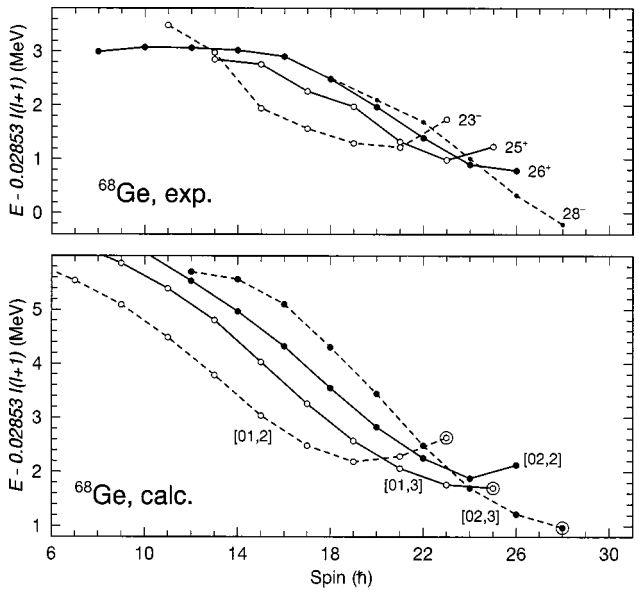

FIG. 6. The observed bands 1–4 in ^{68}Ge (upper panel) and calculated configurations assigned to these bands (lower panel) drawn relative to a rigid rotor reference. The calculated bands are labeled $[p_1p_2,n_1]$ where p_1 is the number of $f_{7/2}$ proton holes and p_2 (n_1) is the number of $g_{9/2}$ protons (neutrons). Calculated terminating states are encircled.

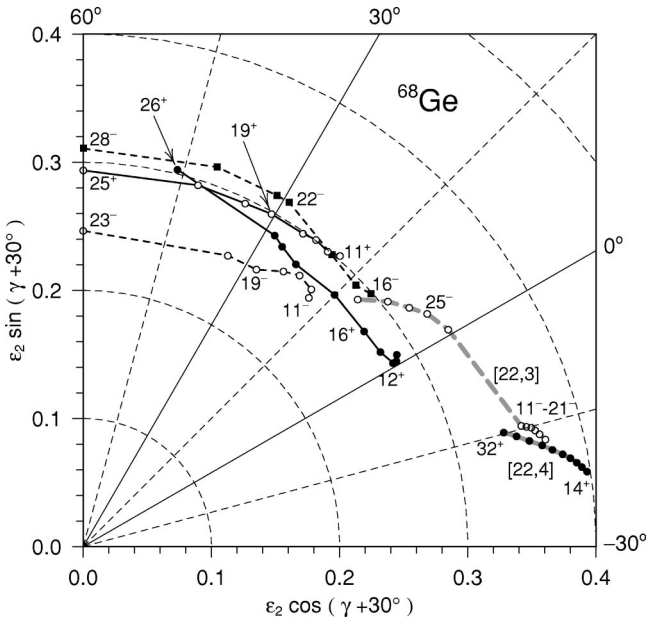

FIG. 7. Shape trajectories in the (ε_2,γ) plane for the four configurations assigned to bands 1–4 in ^{68}Ge and for two configurations with two $f_{7/2}$ proton holes which are possible assignments for the superdeformed band. The configurations are labeled as in Fig. 6.

$$\nu(g_{9/2})^3(f_{5/2},p_{3/2})^5 \Rightarrow I_{\max}=10.5+5.5=16^-.$$

Combining these proton and neutron configurations, we get maximum spin states of 23^-, 25^+, 26^+, and 28^-. These values coincide with the maximum spin states for the observed bands, suggesting that all four of these valence-space bands have been observed to their respective terminations.

B. Comparison of the calculated and observed bands

In Fig. 6, the calculated energy curves (with a rigid-rotor reference subtracted) of the configurations terminating at 23^-, 25^+ and 26^+ and 28^- are compared with the observed bands. The calculated configurations are followed from collective states at low spin and continuously through the γ plane to their termination. In general, there is a good agreement between calculations and experiment.

The shape trajectories of the calculated bands are drawn in Fig. 7. The figure suggests that the 23^-, 25^+, and 28^- states are noncollective terminations and that the 26^+ state is very close to the noncollective oblate axis and can in practice be considered a termination.

As mentioned above, the superdeformed band is expected to have two proton holes in the $f_{7/2}$ subshell. A few low-lying bands of this kind are considered in Fig. 8. They are compared with the superdeformed band assuming different spin values. The comparison indicates that the spins in the band are, if anything, likely to be a few units higher than the preliminary values suggested in Fig. 3. Thus, the observed band is drawn with its lowest spin in the range, $I_0=14-18$. The excitation energy is not known so the experimental curves can only be compared with the slope and the curvature of the calculated configurations, where the curvature, prior to subtracting a reference, is a measure of the $\mathcal{J}^{(2)}$ moment of inertia. The fact that all curves are close to straight lines in the relevant spin range shows that $\mathcal{J}^{(2)}$ is close to the rigid body value at normal deformation, $\varepsilon_2=0.25-0.30$, both in experiment and for the calculated bands. The bands calculated to be lowest at $I\approx 30$ in Fig. 8 are [22,3] and [23,3]. These calculated bands reproduce the experimental band very well if its lowest spin value is chosen as $I_0=17$. For the other two calculated bands in Fig. 8

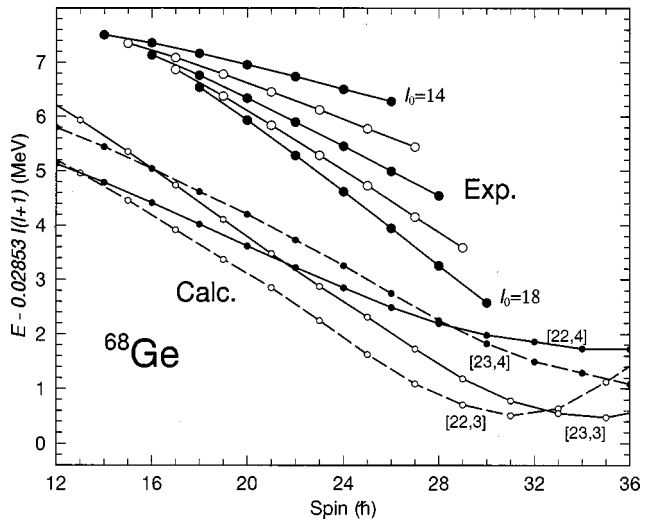

FIG. 8. The superdeformed band with different assumptions about its lowest spin value I_0 and arbitrary excitation energies is compared with a few calculated configurations with two proton holes in the $f_{7/2}$ subshell. The configurations are labeled as in Fig. 6 and the same reference energy is subtracted.

[22,4] and [23,4], the best agreement is obtained if $I_0=16$ or possibly $I_0=14$ for the [22,4] configuration. These latter assignments may at first appear less likely because these bands are calculated higher in energy. However, it is important to note that the superdeformed band observed in ^{62}Zn [1] is assigned [24] to a configuration involving four $g_{9/2}$ neutrons, although this configuration is calculated to be at least one MeV above the superdeformed configuration with two $g_{9/2}$ neutrons in all of Nilsson-Strutinsky, relativistic mean field, and Hartree-Fock calculations [24,25]. This discrepancy is most probably the result of too high an energy for the $g_{9/2}$ orbital in all of the commonly used parameter sets [24,25], so that the higher excitation energy calculated for the ^{68}Ge SD bands with four $g_{9/2}$ neutron intruder orbitals occupied does not rule out these configuration assignments. One might also consider bands with fewer $g_{9/2}$ neutrons than those shown in Fig. 8 as candidates for the superdeformed band. Such configurations, however, tend to build the highest spin states at a high energy cost, i.e., contrary to the observed band they have a small value of the $\mathcal{J}^{(2)}$ moment of inertia at high spin (see Fig. 12 below).

Two typical examples of deformation trajectories for configurations with two proton holes in $f_{7/2}$ are drawn in Fig. 7. In general, the energy minimum is found at a negative value of γ at low and intermediate spin values but the minimum goes over to positive γ values at some spin value, $I=20-35$, depending on the configuration. One can note for example that the small downwards curvature at $I\approx 22$ in the energy of the [22,3] configuration in Fig. 8 is caused by such a shape change while the [22,4] configuration has negative values of γ in the full spin range where the superdeformed band is observed. Thus, this band in ^{68}Ge might be the first case of a superdeformed band built at negative values of γ, i.e., corresponding to rotation around the intermediate axis. However, the evidence that this is indeed the case is far from conclusive.

C. Competition from noncollective states within the calculated configurations

Having made the above interpretations of the observed bands, we note that only smooth calculated configurations have been considered and there are calculated noncollective configurations at lower energies which do not have any counterpart in the observed spectrum.

Let us first illustrate how such states may be formed within the configurations assigned to the observed bands by considering the calculated band terminating at 23^-, which involves the $(g_{9/2})^2(f_{5/2},p_{3/2})^6$ neutron configuration with a maximum spin of $I=8+6=14$. The termination occurs at $\varepsilon_2\approx 0.24$ for the 23^- state. In order to illustrate how this state is built, an e_i vs m_i diagram at this oblate deformation is drawn in Fig. 5. Here, the single-particle energies, e_i depend on the spin projections m_i, and may be represented as points on inverted parabolas in the (e_i,m_i) plane. For oblate deformation, levels with the highest m_i values come lowest in energy. The total angular momentum generated by the particles in the direction of the symmetry axis is just the sum of the relevant m_i values. It is seen that the $I_n=14$ state is not optimal, instead $I_n=12$ and $I_n=8$ optimal states are formed within the $\nu(g_{9/2})^2(f_{5/2},p_{3/2})^6$ configuration. The $I_n=14$ state can then be considered as a particle-hole configuration relative to the $I_n=12$ state as indicated by the dashed line in Fig. 5. When this neutron configuration is combined with the $\pi(g_{9/2})^1(f_{5/2},p_{3/2})^3$ proton configuration which terminates at $I_p=9$ (see the upper panel of Fig. 5) we would expect low-lying 17^- and 21^- states in addition to the 23^- state. This is also seen in the calculations, shown in the lower panel of Fig. 9 where the energy of different local minima of the $\pi(g_{9/2})^1(f_{5/2},p_{3/2})^3$ $\nu(g_{9/2})^2(f_{5/2},p_{3/2})^6\equiv$[01,2] configuration are followed as a function of spin, and compared with the band observed to 23^-.

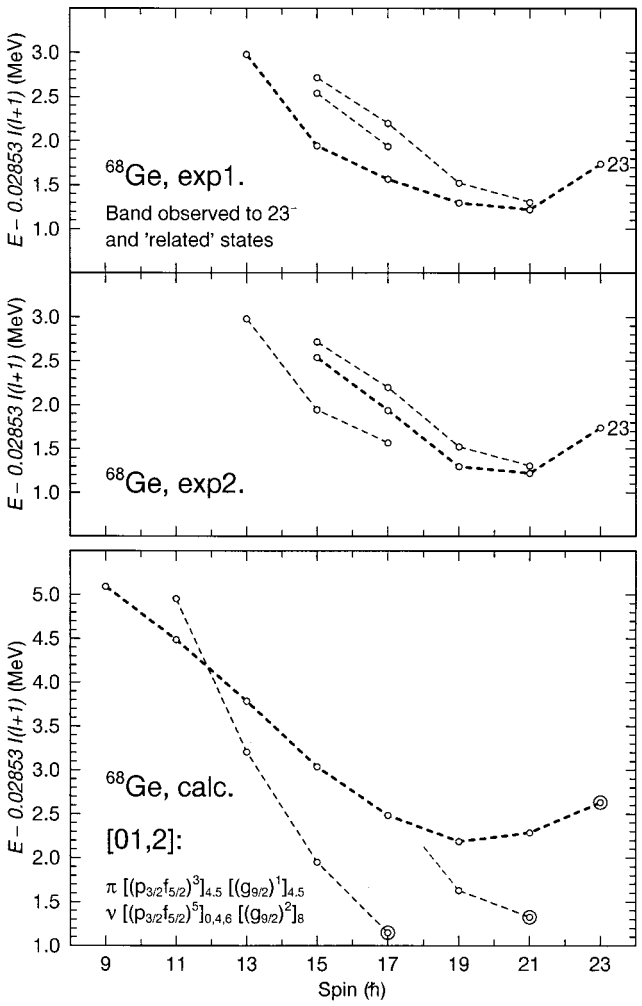

FIG. 9. The calculated ''bands'' of the [01,2] configuration (lowest panel) compared with the observed states of band 1 and other negative parity odd spin states which appear related to this band (upper panels). In the top panel, the observed states are connected to bands as suggested in the level scheme of Fig. 3. The role of the two 17^- states is interchanged in the middle panel, which suggests that the lower 17^- state terminates a band. The coupling of the spin vectors in the encircled aligned states are given in the lower panel and illustrated in an e_i vs m_i diagram in Fig. 5.

As noted above, there is a good agreement between the band calculated to terminate at $I=23^-$ and the band observed to 23^-. However, the calculations suggest other states

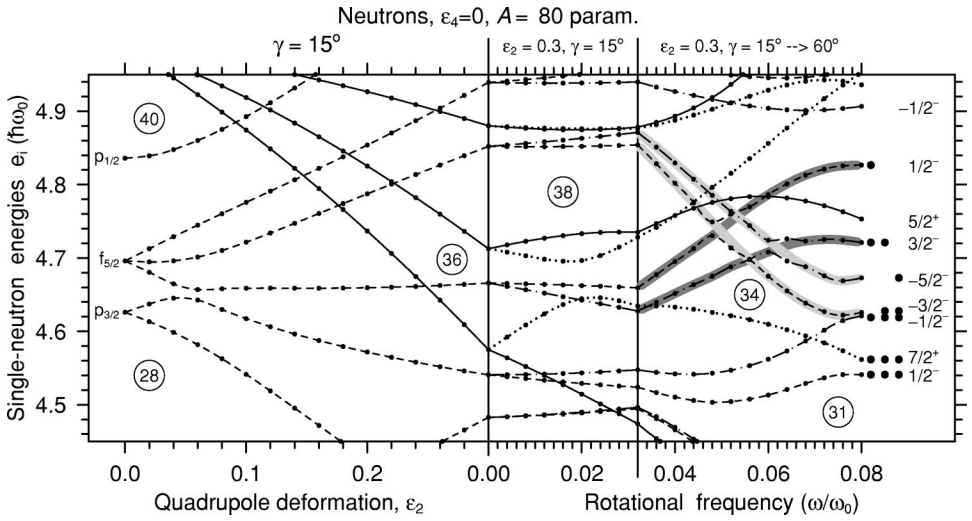

FIG. 10. The neutron orbitals drawn as functions of deformation and rotational frequency to follow the shape evolution of the configuration terminating at $I=23^-$ (and 26^+). At low spin, the deformation of this configuration is $\varepsilon_2\approx 0.30$, $\gamma\approx 15°$ and in the left panel, the spherical origin of the orbitals at this deformation is traced. In the middle panel, the rotational frequency increases at constant deformation while in the right panel, rotational frequency and γ deformation increase proportionally up to the noncollective limit at $\gamma=60°$. The ''rotational frequency'' at this oblate deformation, $\omega/\omega_0=0.08$, corresponds to a sloping Fermi surface in between those defining the 8^+ and 12^+ neutron states in Fig. 5. Filled circles at the right edge indicate which orbitals are occupied in the neutron 14^+, 12^+, and 8^+ states, i.e., the 23^-, 19^-, and 17^- states of the [02,1] configuration and the 26^+, 24^+, and 20^+ states of the [02,2] configuration, respectively.

at 21^- and 17^- which are more favored in energy. These calculated terminating states have a somewhat larger deformation, $\varepsilon\approx 0.30$. Assuming that the calculated bands drawn in Fig. 9 can be assigned to the observed states, there is a substantial discrepancy in the relative energies of the different bands. Analysis of the intensities of the two γ rays depopulating the 19^- state at 12 139 keV indicates that the $B(E2)$ values are nearly equal. This supports the idea that the two 17^- states at 10 668 and 10 297 keV are strongly mixed, and that the observed states could be connected as shown in the middle panel of Fig. 9. Here we indicate that the lowest 17^- state might be considered as a terminating state in agreement with calculation. Most of the disagreement in the relative excitation energies would, however, remain. Concerning this disagreement, one might speculate that there are noncollective states present in the spectrum which have not been observed because they are more difficult to identify experimentally than the cascades of collective transitions.

VI. DISCUSSION OF THE CALCULATIONS

A. Evolution of single-particle orbitals through the γ plane

It is interesting to follow the shape evolution and the orbitals of the [01,2] configuration from low spin to the different aligned states and the final termination at 23^-. For this purpose, Figs. 10 and 11 have been constructed. Starting from a spherical shape, the static orbitals are followed as a

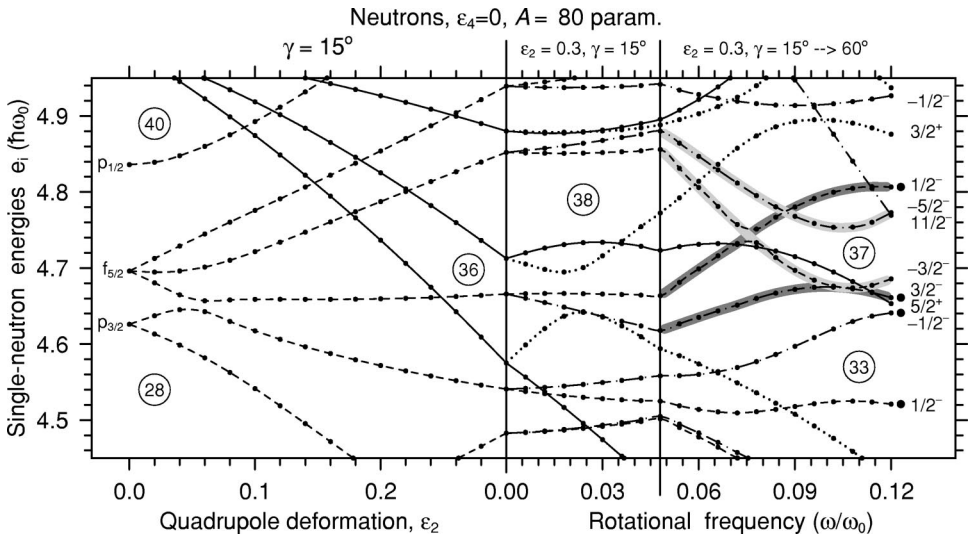

FIG. 11. Similar to Fig. 10, but with a rotational frequency that is 50% larger than in that figure, leading to a ''rotational frequency'' of $\omega/\omega_0=0.12$ at oblate deformation at the right edge, where the orbitals occupied in the neutron 14^+ states are indicated by filled circles.

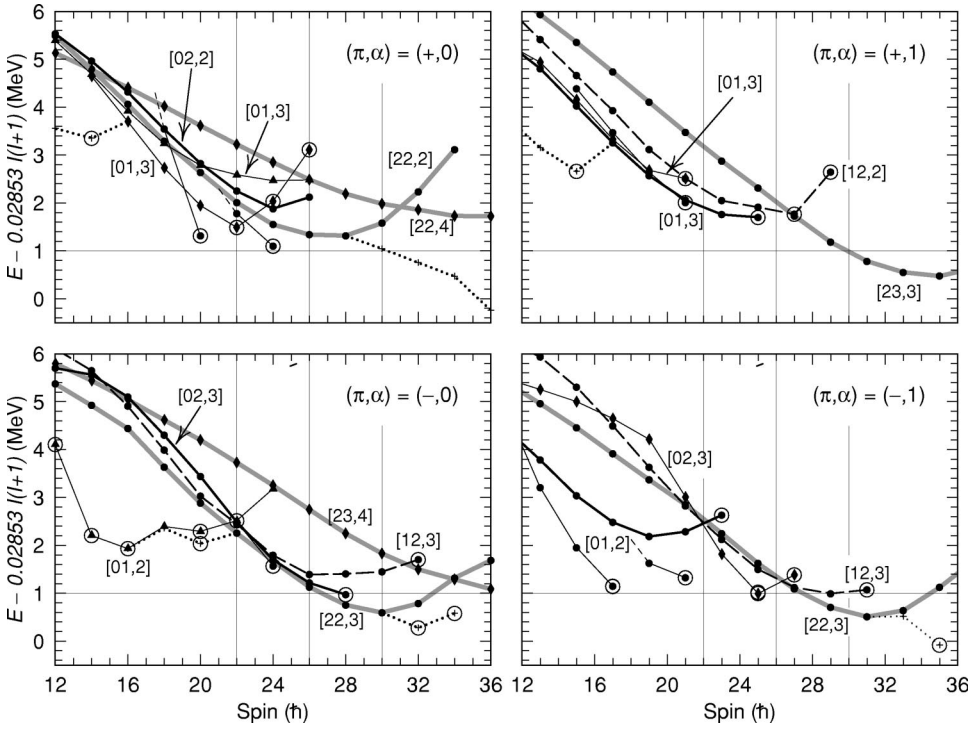

FIG. 12. A selection of calculated low-lying configurations for ^{68}Ge where each panel corresponds to a fixed value of parity and signature. Valence space configurations are drawn by full lines, with thicker lines for those assigned to the observed bands. Dashed lines and thick shaded lines are used for configurations with one and two proton holes in the $f_{7/2}$ subshell, respectively. When the yrast line is not traced it is indicated by a dotted line. Aligned states are encircled. The configurations are labeled as in Fig. 6 and the same reference energy is subtracted.

function of quadrupole deformation to $\varepsilon_2=0.3$ at a ''constant triaxiality'' of $\gamma=15°$. This is a typical low-spin deformation for collective states in the [01,2] configuration. Then the potential is cranked at a fixed deformation up to some intermediate rotational frequency and finally the γ deformation is allowed to increase with a simultaneous increase of the rotational frequency ending up at oblate shape ($\gamma=60°$) at a rotational frequency approximately corresponding to the aligned states discussed above. The only difference between Figs. 10 and 11 is that the rotational frequency is chosen to be 50% larger in Fig. 11 which means that the terminating frequency ($\omega/\omega_0=0.12$) is more appropriate for the 23^- state, while the terminating frequency in Fig. 10 ($\omega/\omega_0=0.08$) is more appropriate for the 17^- state.

Let us first consider Fig. 10. In the middle panel, at $\varepsilon_2=0.3$, $\gamma=15°$, and small rotational frequency the $\nu(g_{9/2})^2(f_{5/2},p_{3/2})^6$ configuration is yrast. Then when going through the γ plane with increasing rotational frequency, two of the ''occupied orbitals'' (dark shaded) go up in energy and meet two ''unoccupied orbitals'' (light shaded), all belonging to the $N=3$ shell and with the same signature in pairs. These orbitals do not interact very strongly so we can either follow the orbitals which are occupied at low spin diabatically to $\gamma=60°$ (dark shading) or we can ''switch'' to the orbitals which come lower at high frequencies and $\gamma\approx 60°$ (light shaded orbitals corresponding to an optimal state at $\gamma=60°$). With the latter orbitals filled the aligned 17^- state is formed while with the former orbitals filled, the aligned 23^- state is formed. This figure suggests that this 23^- is relatively much higher in energy than the 17^- state. With a rotational frequency more appropriate for the 23^- state (Fig. 11), the excitation energy to lift the particles from the light shaded to the dark shaded orbitals at $\gamma=60°$ is smaller, but it is still considerable. With a smaller deformation at termination, the aligned 23^- state will gain some energy relative to the aligned 17^- state, but it will still come relatively higher in energy as seen in Fig. 9. We also note that the 21^- state is formed at $\gamma=60°$ in Fig. 11 if all orbitals below the $N=37$ gap except the $g_{9/2}$, $m_i=5/2$ orbital are occupied.

One might ask if the relative energies of the aligned states at $I=17^-$, 21^-, and 23^- are strongly dependent on the single-particle parameters. No systematic calculations have been carried out to test such a possibility, but preliminary considerations suggest that this is not the case. For a spherical shape, the $p_{3/2}$ subshell is below the $f_{5/2}$ subshell, see Figs. 10 and 11. Even so, at oblate deformations of say $\varepsilon>0.2$, the $N=3$ orbitals come into groups where, starting at low energy, it is tempting to identify them as $f_{7/2}$, $f_{5/2}$, $p_{3/2}$, and $p_{1/2}$, see Fig. 5. This splitting is, however, caused by deformation and it is more appropriate to identify the different groups as being distinguished by n_z, namely $n_z=0$, 1, 2, and 3. Because the splitting is a feature of the deformation, it is expected to be largely independent of the Nilsson κ and μ parameters. In Fig. 5, the orbitals are still labeled by ''$f_{5/2}$'' and ''$p_{3/2}$'' but this is done only to keep track of them without implying any dominating components in their wave functions.

The calculated 23^- terminating state and the associated structures are formed in the [01,2] configuration. Analogous structures with a terminating 26^+ state are formed in the [02,2] configuration where the only difference is that the proton $\pi(g_{9/2})^1(f_{5/2},p_{3/2})^3$ configuration terminating at $I_p=9^-$ has been replaced by the $\pi(g_{9/2})^2(f_{5/2},p_{3/2})^2$ configuration terminating at $I_p=12^+$, see Fig. 5. Consequently, very similar high-spin states are calculated in the [02,2] configuration as in the [01,2], but with all spin values increased by $3\hbar$, see Fig. 12.

B. Favored configurations in the different (π,α) groups

Let us now consider the lowest calculated configurations in general and investigate the energies of the configurations associated with the observed bands relative to other calculated configurations. For this purpose, the lowest energy states for each combination of parity and signature are plotted in Fig. 12. The figure shows that the collective configurations assigned to the observed bands 1–4 (thick black lines), are generally not calculated lowest in energy, but this may largely be the result of the too high energy of the $g_{9/2}$ intruder orbitals mentioned above. It is also interesting to note that for the even-spin, negative-parity states, there are very low-lying aligned 14^- and 16^- states with one $g_{9/2}$ proton and two $g_{9/2}$ neutrons. For the configuration associated with the band terminating at $I=25^+$ [01,3], there is also a shape-coexisting band at approximately the same energy but which terminates at a lower spin of $I=21^+$ and therefore cannot be assigned to the observed band. Another observation is that the configurations with two $f_{7/2}$ holes, [22,2] and [22,3] are close in energy to the configurations [02,2] and [02,3] in the full spin range where these bands are observed. Thus, comparing only energies, these core-excited configurations could be mistakenly assigned to the observed bands. However, the observed properties of bands 1–4 are very different from those of the superdeformed band, and we are led to conclude that bands 1–4 should be assigned to valence space configurations.

VII. SUPERDEFORMED BANDS IN THE $A\sim60-70$ REGION

It is worthwhile to consider the ^{68}Ge superdeformed band in the context of other super-, and strongly-deformed bands which have been observed in the $A\sim60-70$ mass region. The angular momentum versus γ-ray transition energy plots for the SD bands in ^{62}Zn [1], ^{68}Zn [26], and ^{68}Ge (this work) are compared in Fig. 13, where the transition energies for the ^{62}Zn band have been scaled by $(62/68)^{5/3}$ to account for the expected mass dependence of the moment of inertia. Although none of these SD bands have definite spin assignments, and can thus be shifted vertically in Fig. 13, the slopes (dynamic moments of inertia) are clearly very similar in all cases. Lifetimes have been measured for ^{62}Zn [1], and for ^{68}Zn [26], with the result that the deformation $\beta_2\sim0.45$.

Also shown in Fig. 13 are the favored (or possible in the case of ^{68}Ge) configuration assignments for the SD bands, where we use the extended configuration notation $[p_1p_2,n_1n_2n_3]$, where p_1 (n_1) is the number of proton (neutron) $f_{7/2}$ holes, p_2 (n_2) is the number of proton (neutron) $g_{9/2}$ particles, and n_3 is the number of neutron $h_{11/2}$ particles. In all cases shown in Fig. 13, as well as for the superdeformed bands known in ^{60}Zn [3] and ^{61}Zn [5], the SD bands are based on the $p_1p_2=22$ proton configuration corresponding to filling the single-particle energy levels up to the $Z=30$ SD shell gap (plus two extra protons in low-j orbitals above this gap in the case of ^{68}Ge). For $Z<30$, favored collective bands are based on proton configurations obtained by removing particles from the $g_{9/2}$ intruder orbitals, as, for example, in the highly-deformed $p_1p_2=21$ bands in ^{58}Cu [2] and ^{59}Cu [27], and the deformed $p_1p_2=20$ band in ^{56}Ni [4]. In these nuclei, the spin available from the small number of valence particles outside ^{56}Ni is very limited. The deformed bands based on two $f_{7/2}$ proton-hole configurations thus become yrast at relatively low spins and these bands are often populated with a substantial fraction of the channel intensity in high-spin fusion-evaporation reactions. As one moves to $Z>30$ nuclei, breaking the ^{56}Ni core becomes more costly, while, at the same time, the spin available in the valence configurations rapidly increases. The highly-collective bands based on two $f_{7/2}$ proton-hole configurations thus do not become yrast until higher spins and must compete with pure valence space configurations over the feeding region. The observation of the SD band in ^{68}Ge, with only $\sim0.2\%$ of the ^{68}Ge channel intensity, was only possible because of the combination of the very clean selection of ^{68}Ge events and the excellent statistics for this strongly populated reaction channel. Given these considerations, the ^{68}Ge SD band may well represent the high-Z limit of the region of strongly deformed $(f_{7/2})^{-2}$ proton-hole bands which is accessible with current experimental technology.

For the $N=Z$ nuclei in the $A\sim60$ region, the neutron configurations in the strongly deformed bands are, of course, mirrors of the proton configurations. With increasing neutron number, additional neutron $g_{9/2}$ intruder orbitals become occupied. Eventually it is no longer energetically favorable to make holes in the neutron $f_{7/2}$ orbital, as is the case in the ^{68}Ge and ^{68}Zn SD bands. However, the $h_{11/2}$ intruder orbitals, which play a dominant role in the superdeformed bands in the proton-rich $A\sim80$ region, may become occupied. This

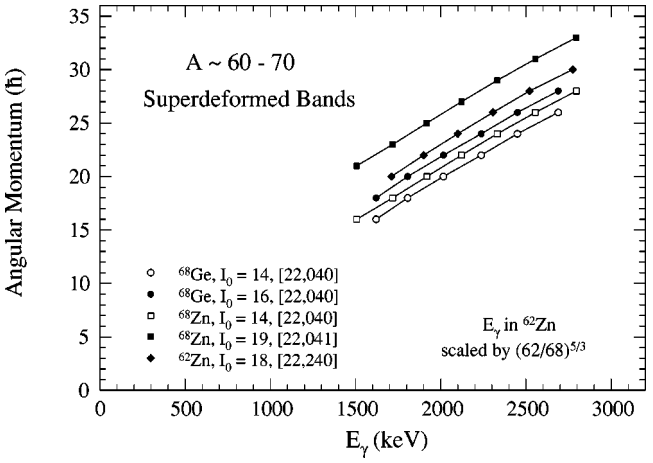

FIG. 13. A comparison of the angular momentum versus γ-ray transition energy plots for the superdeformed bands in ^{62}Zn, ^{68}Zn, and ^{68}Ge. For ^{62}Zn the lowest observed state in the SD band is assumed to have spin $I_0=18$, while for ^{68}Zn and ^{68}Ge the data are shown for $I_0=14$ and $I_0=19$, and $I_0=14$ and $I_0=16$, respectively. For ^{62}Zn the transitions energies have been scaled by $(62/68)^{5/3}$. The bands are labeled by their favored (or possible) configuration assignments with the notation $[p_1p_2,n_1n_2n_3]$, where p_1 (n_1) is the number of proton (neutron) $f_{7/2}$ holes, p_2 (n_2) is the number of proton (neutron) $g_{9/2}$ particles, and n_3 is the number of neutron $h_{11/2}$ particles.

is likely to be the case for the ^{68}Zn SD band [26] shown in Fig. 13, and one may reasonably expect that there will be SD bands in heavier Ge isotopes with the same proton configuration as the ^{68}Ge SD band, but with one or more $h_{11/2}$ intruder orbitals also occupied.

VIII. CONCLUSIONS

The nucleus ^{68}Ge has been studied to high spin. By requiring events with four identified protons, together with a discriminant on the total detected energy, an extremely clean data set was obtained. In cranked Nilsson-Strutinsky calculations, four energetically favored high-spin configurations are identified within the valence space outside the ^{56}Ni core. They involve various numbers of proton and neutron $g_{9/2}$ excitations and give rise to bands terminating at 23^-, 25^+, 26^+, and 28^-, corresponding precisely with the highest spins of the experimentally observed bands. A superdeformed band, populated with $\sim$0.2% of the ^{68}Ge channel intensity, was identified and assigned a configuration in which the ^{56}Ni core has been broken and two protons have been promoted from the $f_{7/2}$ orbital.

ACKNOWLEDGMENTS

We would like to express our gratitude to the crew and staff of ATLAS. This work has been supported in part by the U.S. DOE under Contract Nos. DE-AC03-76SF00098 (LBNL), W-31-109-ENG-38 (ANL), and DE-FG02-88ER-40406 (WU), the Natural Sciences and Engineering Research Council of Canada, the Swedish Natural Science Research Council, EPSRC (U.K.), and BMBF (Germany) under Contract No. 06-OK-668.

[1] C. E. Svensson *et al.*, Phys. Rev. Lett. **79**, 1233 (1997).
[2] D. Rudolph *et al.*, Phys. Rev. Lett. **80**, 3018 (1998).
[3] C. E. Svensson *et al.*, Phys. Rev. Lett. **82**, 3400 (1999).
[4] D. Rudolph *et al.*, Phys. Rev. Lett. **82**, 3763 (1999).
[5] C.-H. Yu *et al.*, Phys. Rev. C **60**, 031305(R) (1999).
[6] A. P. deLima *et al.*, Phys. Rev. C **23**, 213 (1981).
[7] L. Chaturvedi *et al.*, Phys. Rev. C **43**, 2541 (1991).
[8] L. Chaturvedi *et al.*, Int. J. Mod. Phys. E **5**, 1565 (1996).
[9] U. Hermkens *et al.*, Z. Phys. A **343**, 371 (1992).
[10] I.-Y. Lee, Nucl. Phys. **A520**, 641c (1990).
[11] D. G. Sarantites *et al.*, Nucl. Instrum. Methods Phys. Res. A **381**, 418 (1996).
[12] M. Devlin *et al.*, Nucl. Instrum. Methods Phys. Res. A **383**, 506 (1996).
[13] C. E. Svensson *et al.*, Nucl. Instrum. Methods Phys. Res. A **396**, 228 (1997).
[14] D. Seweryniak, J. Nyberg, C. Fahlander, and A. Johnson, Nucl. Instrum. Methods Phys. Res. A **340**, 353 (1994).
[15] D.C. Radford, Nucl. Instrum. Methods Phys. Res. A **361**, 297 (1995).
[16] D. Ward *et al.*, Nucl. Phys. **A529**, 315 (1991).
[17] http://radware.phy.ornl.gov/nd/68Ge_dw.dat
ftp://radware.phy.ornl.gov/pub/nd/68Ge_dw.dat
[18] A. Petrovici *et al.*, Nucl. Phys. **A483**, 317 (1988); **A504**, 277 (1989); **A517**, 108 (1990).
[19] M. E. Barclay *et al.*, J. Phys. G **12**, L295 (1986).
[20] V. V. Afanasjev, D. B. Fossan, G. J. Lane, and I. Ragnarsson, Phys. Rep. **332**, 1 (1999).
[21] I. Ragnarsson and A. V. Afanasjev, Proceedings of the Conference on Nuclear Structure at the Limits, Argonne, ANL/PHY-97/1, 1997, p. 184.
[22] H. Sun *et al.*, Phys. Rev. C **59**, 655 (1999).
[23] D. Galeriu *et al.*, J. Phys. G **12**, 329 (1986).
[24] A. V. Afanasjev, I. Ragnarsson, and P. Ring, Phys. Rev. C **59**, 3166 (1999).
[25] H. Madokoro and M. Matsuzaki, Prog. Theor. Phys. **101**, 1027 (1999).
[26] M. Devlin *et al.*, Phys. Rev. Lett. **82**, 5217 (1999).
[27] C. Andreoiu *et al.*, Phys. Rev. C (to be published).